https://doi.org/10.20965/ijat.2018.p0622

Paper:

Efficient Static and Dynamic Modelling of Machine Structures with Large Linear Motions

Natanael Lanz*,†, Daniel Spescha, Sascha Weikert**, and Konrad Wegener***

*Institute of Machine Tools and Manufacturing (IWF), ETH Zürich
Leonhardstrasse 21, 8092 Zürich, Switzerland
†Corresponding author, E-mail: lanz@iwf.mavt.ethz.ch
**inspire AG, Zürich, Switzerland

[Received November 15, 2017; accepted August 7, 2018]

Mechatronic structures deform under static and dynamic loads. These deformations lead to deviations at the tool center point (TCP), affecting the reachable accuracy and/or productivity of the machines. The scope of this work is the comparison of calculations and measurements of different static and dynamic errors on a dynamic test bench. A reduced-order modelling approach is applied for the test bench modelling. It uses a combination of modal condensation and moment-matching methods with Krylov subspaces. The different modelling steps and requirements are presented. The same model is used for all static and dynamic evaluations presented within this paper. Static deformations, leading to roll and pitch deviations at the TCP of the test bench structure, are simulated using the described modelling methodology and validated by inclination measurements. The modal behavior of the system is investigated by calculation and compared to the measurements at a single axes position. The spatial change of the frequency response functions of the modelled system is investigated further, by calculation and measurement of the velocity open-loop FRFs of one axis for different machine configurations. In addition, a transient trajectory simulation is performed and compared to the Heidenhain KGM and encoder measurements. The large variety of comparisons shows the efficient applicability of the modelling environment MORe.

Keywords: machine dynamics, modelling, measurements, control

1. Introduction

Mechatronic structures deform under gravitational and dynamic loads. These deformations lead to deviations at the tool center point (TCP). The scope of this work is the efficient simulation and accurate measurement of different static and dynamic errors.

For the prediction of the accuracy and performance of mechatronic systems in terms of static and dynamic structural deviations, efficient and accurate simulation is required. Therefore, in [1], a new modelling procedure, using reduced-order FE-models with Fourier interface coupling is implemented into a software environment named MORe [2]. A combination of modal condensation techniques [3] and moment-matching Krylov-subspace methods [4] is used to reduce the model order of each structural component of the FE-model.

In contrast to the parabolic approach, proposed in [5], a new Fourier-series approach is used for the coupling of the reduced order FE-elements.

Based on and in addition to the static roll and pitch angle calculations and measurements presented in [6], measurements and simulations of the modal structure behavior, spatial frequency response functions (FRFs), and transient motions are shown for the example of a gantry test bench system.

2. Modelling Methodology

Machine tool structures basically have similar static and dynamic properties, which are:

- large linear and rotational motions.
- small deformations compared to the motion range.
- limited excitation frequency range.

All these properties have to be represented by an appropriate machine model. Further, they might be taken advantage of in order to derive a more efficient and accurate modelling procedure. For this, in [1], a modelling framework called MORe [2] was presented; it is used for the machine model derived within this work. MORe uses reduced-order FE-models with Fourier-interface coupling and basically contains four model elements: components, interfaces, links, and composition; these are explained further in the following sections.

2.1. Components

Each component is a single reduced-order FE-model representing a structural machine element such as the machine bed or mass (e.g., table) moved by an axis. In addition, the rotor of a motor or the spindle of a ball-screw drive are represented as components. The software Ansys® was used for the component meshing and export of the original size FE-mass and stiffness matrices.

In MORe, the order of the component's original large-scale mass and stiffness matrices is reduced using modal condensation and Krylov subspace methods. Krylov subspace reduction is used with a single expansion point at the static frequency of $\omega = 0$ rad/s to ensure correct computation of the structural deformation under static load. In addition, modal condensation is used to represent the dynamic structural stiffness, by introducing all natural frequencies up to a definable threshold maximum frequency ω_r into the reduction basis.

Therefore, the dynamics of each component $\mathbf{i}$ is represented by its reduced order mass $\mathbf{M_r^i}$, damping $\mathbf{D_r^i}$, and stiffness matrix $\mathbf{K_r^i}$:

$$\mathbf{M_r^i} \cdot \ddot{\mathbf{q}}^\mathbf{i} + \mathbf{D_r^i} \cdot \dot{\mathbf{q}}^\mathbf{i} + \mathbf{K_r^i} \cdot \mathbf{q^i} = \mathbf{F^i} \quad (1)$$

where $\mathbf{q^i}$ and $\mathbf{F^i}$ are the model states vector and external force input vector, respectively.

For detailed information regarding the mathematical formulation of the reduction algorithm used in MORe, refer to [1, 7].

The reduced system has been shown to represent the original component's behavior within a predictable error bound in [1] if the excitation and response frequencies in the range of 0 to (ω_r/κ) are considered, where $\kappa > 1$ denotes the frequency range restriction factor [7]. This factor needs to be introduced, because natural frequencies slightly above ω_r affect the reduction error negatively around this frequency. Furthermore, the error at the eigenvalues of the original systems are matched exactly by the modal condensation, which means that the error is zero at these specific frequencies.

To define ω_r one needs to measure or estimate the maximum excitation frequency of the system, resulting from either the axes motion, the process, or external perturbations such as floor vibrations.

2.2. Interfaces

Interfaces define all local regions (faces) on a component, where either a force is applied or a position/velocity/acceleration is read. Interfaces represent the system inputs and outputs. The input vector $\mathbf{u^i}$ of interface i can be interpreted as the averaged force and torque component acting on the interface in up to six directions, whereas the output vector $\mathbf{x^i}$ denotes the averaged linear or rotary displacement of the interface nodes. The inputs and outputs are represented by the the input matrix $\mathbf{B_r^i}$ and output matrix $\mathbf{C_r^i}$, respectively:

$$\mathbf{F^i} = \mathbf{B_r^i} \cdot \mathbf{u^i} \quad (2)$$

$$\mathbf{x^i} = \mathbf{C_r^i} \cdot \mathbf{q^i} \quad (3)$$

where $\mathbf{B_r^i}$ is the component interface input matrix, $\mathbf{C_r^i}$ the output matrix, $\mathbf{q^i}$ the system states and $\mathbf{F^i}$ the states input vector. For guaranteed stability after reduction of an

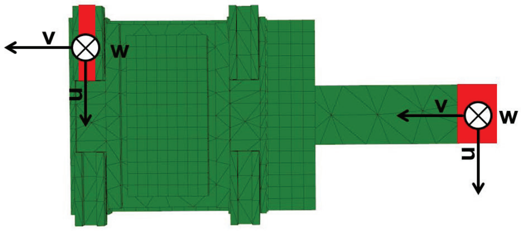

Fig. 1. Two stationary interfaces (guiding slide and TCP) with corresponding local coordinate system $\mathbf{u}, \mathbf{v}, \mathbf{w}$.

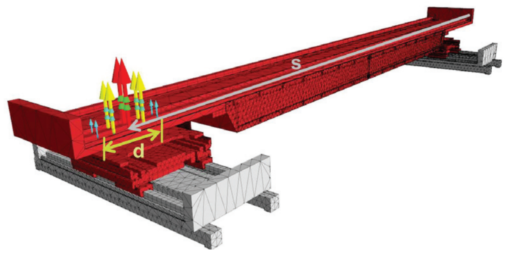

Fig. 2. Moving Fourier interface on a rail at path position s with trapezoidal force distribution width d.

originally stable large system [8] there cannot be any distinction between the input and output. Therefore the following holds:

$$\mathbf{C_r^i} = \mathbf{B_r^i}^\mathbf{T}, \quad (4)$$

where each column of $\mathbf{B_r^i}$ represents one single interface input or output nodal weighting vector. All interfaces have their own local coordinate system $\mathbf{u}, \mathbf{v}, \mathbf{w}$. The interface weighting matrices $\mathbf{B_r^i}$ are used for the Krylov subspace reduction, and its size (number of columns) is a lower bound for the reduced component reachable minimum order. Each interface has up to six degrees of freedom (DOFs), each represented by a column in $\mathbf{B_r^i}$.

Two different types of interfaces are introduced:

- Stationary interfaces with up to six DOFs.
- Moving Fourier interfaces with up to six DOFs.

Stationary interfaces are used if the interface location is not moving relatively to the component. As an example, **Fig. 1** shows two stationary interfaces for one guiding slide and the tool center point (TCP) on a machine component with their corresponding local coordinate systems. The guiding slide interface is used as the force input for the flexible connection of the component to the rail. The TCP interface is used to read its position and velocity.

In contrast, moving interfaces are used if the interface position moves relative to the corresponding component, as it is needed for the connection of the guiding slide to the corresponding rail. As an example, **Fig. 2** shows a moving interface on a guiding rail at an arbitrary path position s. For the moving interface definition with total path length L, a Fourier series of sinusoidal force input signals

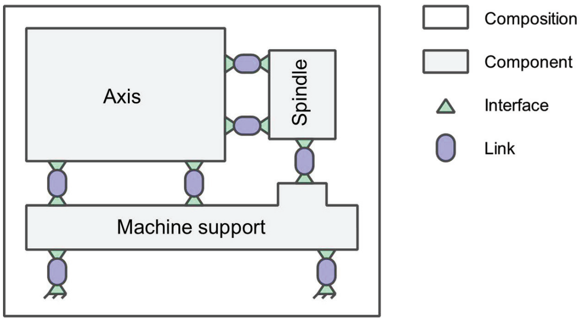

Fig. 3. Composition: assembled system matrices using information from components, interfaces, and links.

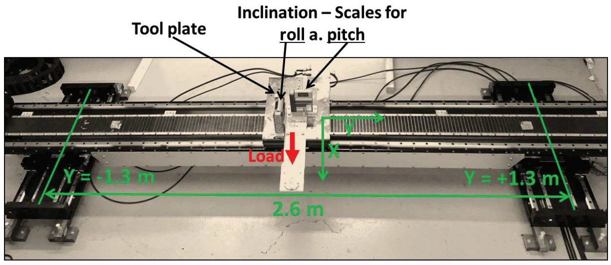

Fig. 4. Linear gantry stage test bench used for static and dynamic modelling and measurements.

Table 1. Test bench mechanical properties.

	$X1$- and $X2$-Axes	Y-axis
Motion range	0.38 m	2.6 m
Kinematic configuration	Gantry	Single motor
Moving mass	210 kg	39.2 kg

with N harmonics is used to approximate a trapezoidal force distribution with base length d, where it holds that:

$$d \approx \frac{L}{N} \quad (5)$$

2.3. Links

Links represent the possible interactions between two interfaces. The following three types of links exist:

- Output link: This link is used to read out the relative position, velocity or acceleration between two interfaces in local coordinates and in up to six DOFs. Example: reader head of a linear scale.
- Input link: This link is used to give an action and reaction force between two interfaces. Example: force applied by a direct drive.
- Linear-elastic damping and stiffness link: This link is used for the modelling of linear-elastic coupling and linear velocity-dependent damping between two interfaces or the ground. Example: elastic coupling of guiding slide and rail.

2.4. Composition

In the composition, the overall reduced-order mass, stiffness, and damping matrices were calculated using all the information from the interface definitions and the links to represent the assembled system behavior. **Fig. 3** schematically shows an example composition for a system with three components, 12 interfaces and seven links.

3. Linear Gantry Stage

A linear gantry stage is used as the test bench for the measurements and simulation.

3.1. Test Bench

The presented modelling procedure was applied to the linear gantry stage shown in **Fig. 4**. The stage consists of an X-axis in gantry configuration with $X1$- and $X2$-motors, and a Y-axis mounted on the bridge between the X-motors. All the motors are linear drives from the company ETEL.

The mechanical properties of the test bench are summarized in **Table 1**. The gantry stage is controlled using a MATLAB/Simulink® interface to the drives for tracking control.

3.2. Test Bench Model

To apply the modelling methodology described in Section 2, CAD data was derived by geometrical measurements of the test bench components as the first step. In the second step, the CAD data was used to generate FE-models of each component and to export the corresponding component mass and stiffness matrices to MORe.

Table 2 lists all the model components and their original and reduced DOFs. The assembled composition has a reduced order of 482, including 30 stationary interfaces and 12 moving interfaces as the input for the model order reduction algorithm.

Stationary interfaces are defined at the eight stage-mounting points, each guiding slide (four per motor), the reader heads (one per motor), motor electromagnets (one per motor), load acting position, inclination measurement positions, and the TCP.

Moving interfaces are defined on each rail, along the three optical axis measurement scales and along the permanent magnet paths, as the motor force is assumed to act on the magnets.

It is assumed that the maximum excitation bandwidth is not higher than ten times the controller bandwidths of approximately $f_c = 30$ Hz. Therefore, the model is reduced to:

$$f_r = 10 \cdot f_c = \frac{\omega_r}{2\pi} = 300 \text{ Hz} \quad (6)$$

The maximum relative error bound for the model order reduction is set as 5%.

This model was used for all further static, dynamic, and position-dependent simulations detailed in this paper.

Table 2. Test bench FE-model components and their original and reduced model orders. Modal reduction limit frequency $f_r = 300$ Hz.

$f_r = \dfrac{\omega_r}{2\pi} = 300\,\text{Hz}$	**Component**	**DOF's original**	**DOF's reduced**
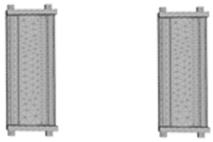	$X1$ & $X2$-bodies	98.598	224
	X-bridge	292.869	412
	Y-slide	42.510	49
Total		**433.977**	**685**

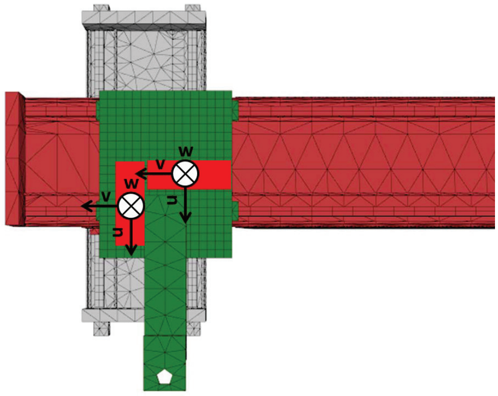

Fig. 5. Interfaces at the inclination sensor positions with corresponding local coordinate system **u**, **v**, **w**.

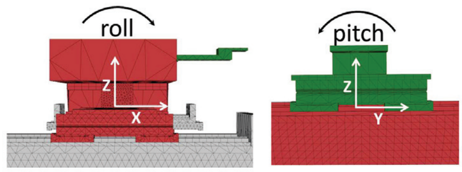

Fig. 6. Roll (right) and pitch (left) angle directions.

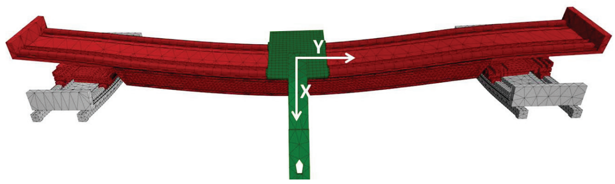

Fig. 7. Deformed test bench under gravitation only (0 kg) at the center position; scaling factor 750.

4. Static Deformations Under Gravitational Load

Using the presented test bench and model, the static deformations of the test bench structure under gravitational load at different positions along the Y-axis were simulated and measured. The simulation and measurement procedure and results are described in this section.

4.1. Experiment

An experiment was performed to measure and simulate the static deformation of the test bench, exposed to gravitation and additional loads. Therefore, the Y-slide was therefore moved in 5-cm steps from -1.3 m to $+1.3$ m three times: the first time without any additional load, the second time with 18 kg of additional load at the position indicated by the red arrow in **Fig. 4**, and the third time with 58 kg of additional load; this is a total of 53 positions for each load case.

4.2. Simulation Procedure

To set up the simulations, the positions of the two inclination measurement sensors are defined as interfaces in the model as shown in **Fig. 5**.

Simulations were performed for all three load cases of 0, 18 and 58 kg of additional load at 53 different Y-axis positions. The Y-axis roll (tilt angle around Y) and pitch (tilt angle around X) were evaluated at each position and for every load case. The total computation time for all positions and load cases is below 1 min on a standard desktop work station with 8 CPU's and 32 GB of RAM.

4.3. Measurement Procedure

For the measurements, the inclination sensors were placed on the Y-slide as indicated in **Fig. 4**. Two WYLER BlueLevel inclination sensors [9] were used simultaneously to measure pitch and roll angle of the Y-slide at all 53 Y-positions and for all three load cases. The sensitivity of the sensors is at 0.001 mm/m according to the manufacturer.

In **Fig. 6**, the rotational positive directions of the inclination deviations for roll and pitch are shown in the corresponding reference plane.

Each measurement was performed multiple times. However, the repeated measurement results did not exceed a significant variation, and thus one representative result was used for the evaluation.

4.4. Results of Static Evaluations

Figure 7 shows the simulated structural static deformation for the 0 kg load case at the center position, scaled with a factor of 750. **Fig. 8** shows the pitch and roll tilt angles for the simulation **(a)** and the measurements **(b)**. It

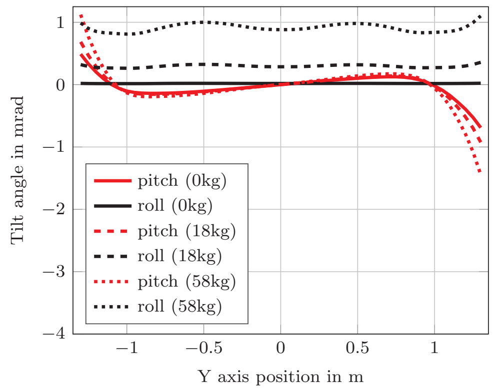

(a) Simulation results

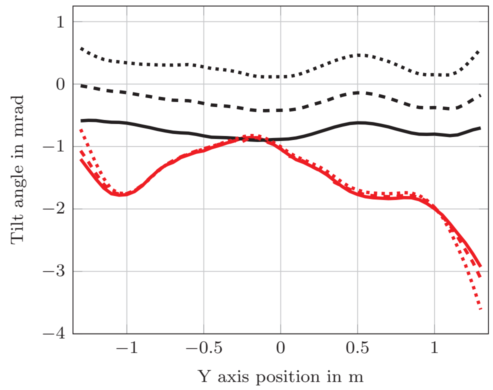

(b) Inclination measurement results

Fig. 8. Results of pitch and roll angle measurements and simulations without reference (raw).

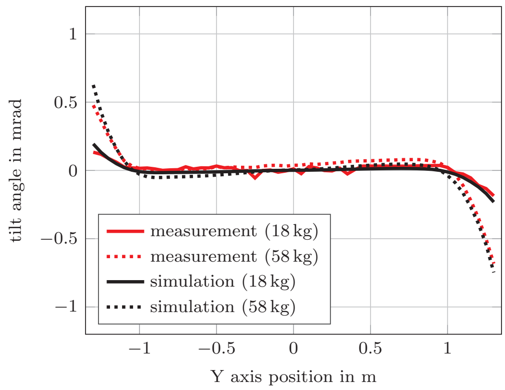

(a) Pitch angle

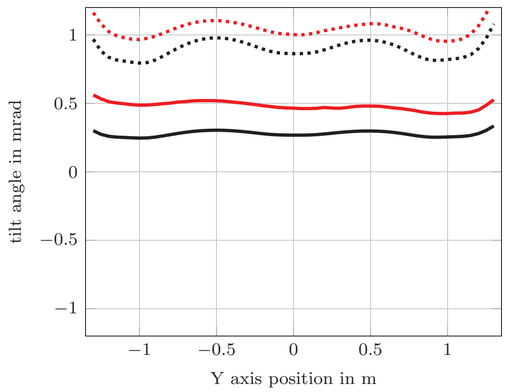

(b) Roll angle

Fig. 9. Tilt angle comparison between measurements and simulation with load case 0 kg as reference.

is obvious that the measurements differ significantly from the simulations, as they include the geometrical errors of the stage (e.g., straightness), which cannot be included in the simulation. Therefore, the measurement with no additional load was chosen as the reference, to remove the geometrical error influence.

Figures 9(a) and **(b)** compares the measurements and results of the pitch and roll angles, respectively, for the load cases of 18 kg and 58 kg by subtracting the results from the 0 kg load case.

4.5. Conclusion of the Static Evaluations

For the presented test bench, the geometrical straightness errors of the rails in the Y-direction are in the same range as the static deformations due to gravitational load. Removing the effect of the geometrical errors by using the 0 kg load case as the reference, the results of the pitch angles for increasing loads show a very good match between the simulation and measurement, as shown in **Fig. 9(a)**.

Greater deviations exist between the measurements and simulations for the roll angle in **Fig. 9(b)**. It is assumed that the constant offset between the measured and simulated roll angle is caused by some sort of backlash phenomenon, which appears when the additional load is applied, especially because the offset is similar for both 18 kg and 58 kg load cases. Nevertheless the local stiffness changes along the Y-axis, resulting in a wave form, is simulated with high accuracy.

Therefore, the results show that the presented modelling and simulation tool can be used for the efficient and accurate modelling of the presented load cases.

5. Modal Analysis

A modal analysis was performed using the presented test bench and its static and dynamic model.

5.1. Analysis Procedure

A modal analysis was performed, using the reduced-order mass and stiffness matrices of the test bench model. Therefore, the natural frequencies were calculated by computing the modes (eigenvalues) and mode-shapes (eigenvectors) of the reduced-order system. This was conducted using the center position of the X- and Y-axes for a later comparison with an experimental modal analysis.

The computation time for solving the modal analysis is below 2 s.

5.2. Measurement Procedure (EMA)

For the comparison of the numerical modal analysis results, an experimental modal analysis (EMA) was per-

Table 3. Comparison of results of EMA and the calculation.

Mode No.	Description	Frequency EMA	Frequency Calculation
1	Bending of X-bridge around X	36.8 Hz	36.0 Hz
2	Movement of X-bridge in Y-direction, wing mode $X1$	41.8 Hz	39.6 Hz
3	Movement of X-bridge in Y-direction, wing mode $X2$	48.9 Hz	46.3 Hz
4	Movement of X-bridge in Y-direction, wing mode $X1$ and $X2$	52.4 Hz	49.0 Hz
5	Rotation of X-bridge around (pitch) Y	58.5 Hz	59.4 Hz
6	Bending of X-bridge around Z	131.8 Hz	119.9 Hz
7	Two bendings of X-bridge around X	119.9 Hz	119.0 Hz

formed on the test bench, also at the center positions of all axes. For this, 3D PCB accelerometers were placed at 48 different points on the test bench. A hammer pulse was used for the test bench excitation. The resulting measured modes and mode shapes were estimated by calculating the frequency response functions (FRFs) from the hammer pulse signal to the 3D acceleration sensor signals and applying a mode-fit. A sampling frequency of 1500 Hz was used.

5.3. Results of Modal Evaluations

The first seven modes and mode shapes with their corresponding frequencies and description are shown as a comparison between the measurement and calculation in **Table 3**. **Table 4** shows a graphical representation of the described modes together with the relative errors between the measured and calculated natural frequencies.

5.4. Conclusion of Modal Evaluations

The simulation and measurement results of the test bench modal analysis show, that the presented modelling methodology is capable of computing the mode frequencies and shapes with a relative error below 10%. An error in this range, can also be expected if full order models are used. This indicates that reduced-order models can be used to increase the computation efficiency dramatically, for modal simulations, without a significant loss in accuracy.

6. Position-Dependent FRFs

As the dynamics of machine structures may be highly dependent on the positions of the axes, it is important

Table 4. Graphic representation of the comparison between the modes and mode shapes determined via EMA and the calculation.

Mode No. Rel. error	**Measurement** Shape Frequency	**Calculation** Shape Frequency
1		
−2.2%	36.8 Hz	36.0 Hz
2		
−5.3%	41.8 Hz	39.6 Hz
3		
−5.2%	48.9 Hz	46.3 Hz
4		
−6.4%	52.4 Hz	49.0 Hz
5		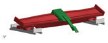
1.4%	58.5 Hz	59.4 Hz
6		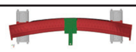
−9.1%	131.8 Hz	119.9 Hz
7	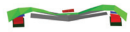	
−5.3%	119.9 Hz	119.0 Hz

to be able to characterize the structural behavior in the frequency domain throughout the work space. Therefore open-loop FRFs were computed by simulation and measurement for the $X1$- and $X2$-axes of the test bench, while moving the Y-axis to 27 different positions in total. The results of these two approaches are compared in this section.

6.1. Analysis Procedure

The velocity open-loop FRFs of the $X1$- and $X2$-axes were computed at 27 positions in total, using the model presented in Section 3.2.

The required total calculation time could be maintained at at less than 10 s, due to the low model order.

6.2. Measurement Procedure

The velocity open loop FRFs were also measured at the same 27 axis positions using a sinusoidal chirp excitation reference trajectory. According to [10], the velocity gain was set to optimally damp the bandwidth-limiting first dominant natural frequency in the X-direction (Mode No.5 in **Table 4** at 58.5/59.4 Hz, measurement/simulation).

6.3. Results of FRF Evaluations

The simulated **(a)** and measured **(b)** velocity open-loop spatial surface FRFs at the 27 different Y-positions are shown in **Figs. 10** and **11** for the $X1$ and $X2$ motors, respectively. The amplitude is indicated by different shades of gray.

6.4. Conclusion of FRF Evaluations

For dynamic systems, such as mechatronic machine structures, the lowest natural frequency in the axis direction limits the reachable control bandwidth and is therefore responsible for the reachable tracking accuracy. As described, the limiting natural frequency for the two X-motors ($X1$ and $X2$) of the test bench is Mode No.5 in **Table 4**. This resonance mode (first bright line) and its change in the Y-position is represented very accurately for both the $X1$ and $X2$ motors in **Figs. 10** and **11**, respectively. The anti-resonance frequency in front of the resonance (first dark line) approaches the resonance frequency as the Y-axis moves towards the corresponding X-motor. This behavior is represented in the simulation as well as in the measurements.

The higher modes are slightly shifted in the simulation compared to the measurement; however, their spatial changing behavior is represented well in simulation compared to the measurements.

7. Transient Motions

A reduced-order model enables transient system simulations, and this is used to obtain information about the deviation on the encoder level as well as at the TCP. Therefore, an example 2D trajectory was simulated and measured.

7.1. Motion Control Parametrization

A proportional cascaded loop velocity and position controller without feed forward was used for axes control. As aforementioned, the velocity gain was parametrized to optimally damp the first natural frequency in corresponding axis directions according to the theory presented in [10]. The position gain of the Y-axis was adjusted, such that the position loop damping was $1/\sqrt{2}$. The X-axis position gain was set to the same value as the Y-axis position gain to synchronize the axes correctly according to [11].

7.2. Simulation Procedure

The MORe MATLAB/Simulink® interface was used for the simulation. Therefore, the dynamic test bench model was introduced into a closed loop Simulink® model. The controller gains were chosen identical to those used for the measurements on the test bench. The same reference trajectory was used as model input as for the measurements. The model was evaluated at encoder and TCP level. The simulation time for the trajectory lasting 4.5 s in reality was below 1 min.

7.3. Measurement Procedure

A Heidenhain KGM was used for the TCP-position measurements, as well as the $X1$-, $X2$-, and Y-encoder measurements. The sampling frequency was chosen to be 1 kHz according to the sampling frequency of the drive.

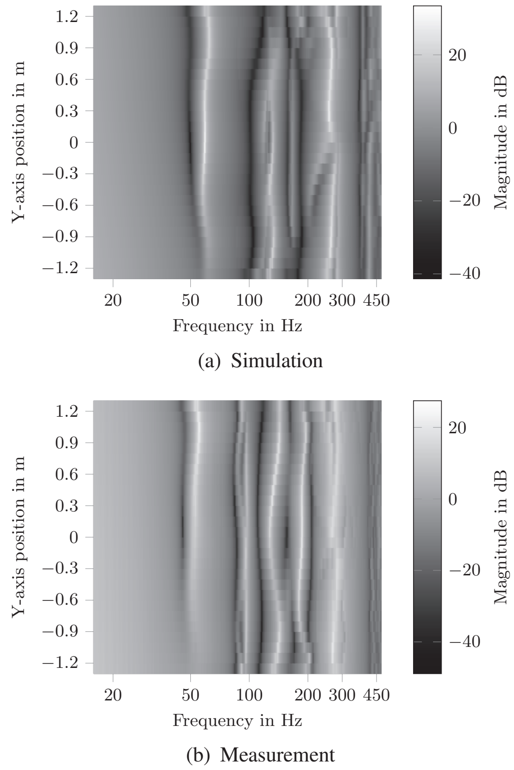

Fig. 10. $X1$ motor open-loop velocity FRFs (gray shaded magnitude) for 27 Y-axis positions between −1.3 m and +1.3 m.

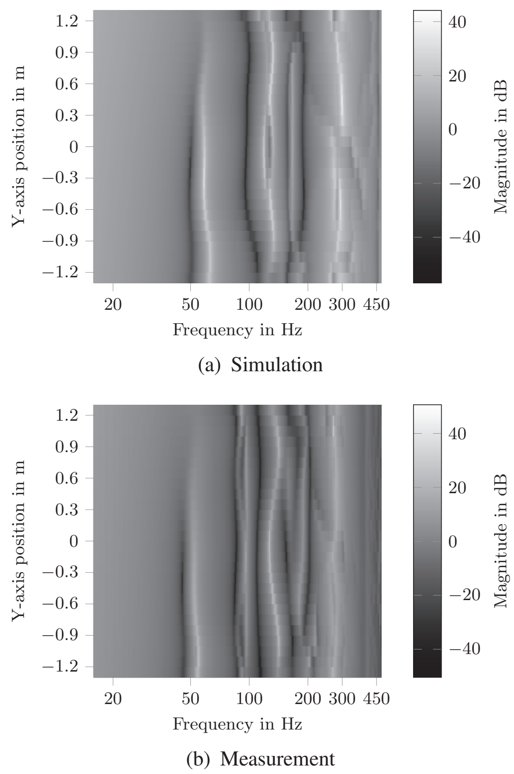

Fig. 11. $X2$ motor open loop velocity FRFs (gray shaded magnitude) for 27 Y-axis positions between −1.3 m and +1.3 m.

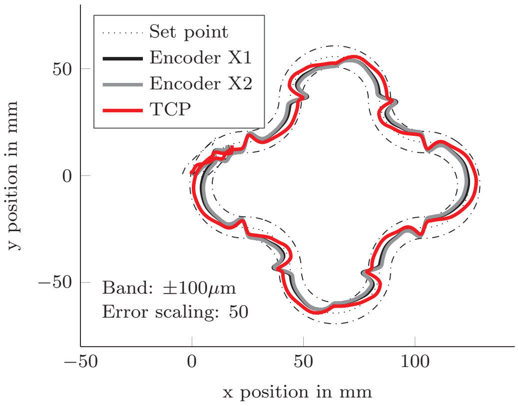

(a) Simulation

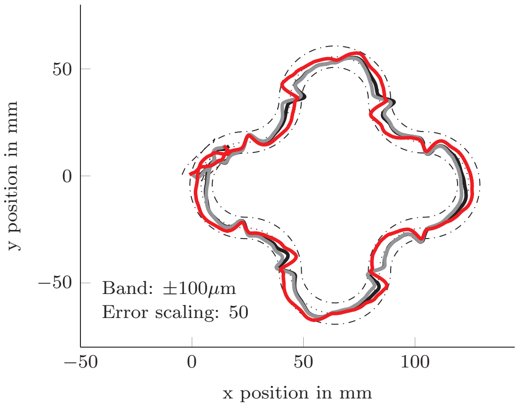

(b) Measurement

Fig. 12. Transient simulation and measurement of an example test bench trajectory.

7.4. Results of Transient Evaluations

Figure 12 shows the results of the transient simulation **(a)** and measurement **(b)** with a trajectory error scaling of 50.

7.5. Conclusion

The simulation and measurement trajectory error show a similar behavior and value at both the encoder and TCP levels. In particular, the difference between the motion of the motors at the encoder level and the motion at the TCP level are well-described by the model and the simulation results. Therefore, it is shown that transient simulations with reduced-order models may reasonably be used for transient machine system evaluations.

References:

[1] D. Spescha, "Framework for Efficient and Accurate Simulation of the Dynamics of Machine Tools," Ph.D. thesis, Technische Universität Clausthal, 2018.

[2] D. Spescha, "More Software," 2017. https://www.more-simulations.ch/ [Accessed August 24, 2018]

[3] J. Berkemer, "Gekoppelte Simulation von Maschinendynamik und Antriebsregelung unter Verwendung linearer Finite Elemente Modelle," Ph.D. thesis, Institut für Statik und Dynamik der Luft- und Raumfahrtkonstruktionen, Universität Stuttgart, 2003.

[4] S. B. Salimbahrami, "Structure preserving order reduction of large scale second order models," Ph.D. thesis, Universität München, 2005.

[5] D. Siedl, "Simulation des dynamischen Verhaltens von Werkzeugmaschinen während Verfahrbewegungen," Ph.D. thesis, Institut für Werkzeugmaschinen und Fertigung, Technische Universität München, 2008.

[6] N. Lanz, D. Spescha, N. Ceresa, A. Ryser, and S. Weikert, "Modelling and Validation of Position Dependant Structural Deformations of a Machine Tool Structure under Gravitational Loads," euspen 17th Int. Conf. & Exhibition, 2017.

[7] D. Spescha, S. Weikert, S. Retka, and K. Wegener, "Krylov and Modal Subspace based Model Order Reduction With A-Priori Error Estimation," ETH Zürich Research Collection, doi: 10.3929/ethz-b-000284435, 2018.

[8] B. Salimbahrami, R. Eid, and B. Lohmann, "Model reduction by second order Krylov subspaces: Extensions, stability and proportional damping," Proc. of the 2006 IEEE Conf. on Computer Aided Control Systems Design, CACSD, pp. 2997-3002, 2007.

[9] "Whyler Blue Level," 2017. https://www.wylerag.com/ [Accessed August 24, 2018]

[10] O. Zirn, "Machine tool analysis – modelling, simulation and control of machine tool manipulators," A Habilitation Thesis, ETH Zürich, 2008.

[11] D. Spescha, S. Weikert, O. Zirn, and K. Wegener, "Synchronisation of feed axes with differing bandwidths using set point delay," Int. J. Automation Technol., Vol.11, No.2, pp. 155-164, 2017.

Name:
Natanael Lanz

Affiliation:
Research Assistant, Institute of Machine Tools and Manufacturing (IWF), ETH Zürich

Address:
Technoparkstrasse 1, 8005 Zürich, Switzerland

Brief Biographical History:
2012 Received Bachelor of Science from Mechanical Engineering, ETH
2014 Received Master of Science from Mechanical Engineering, ETH
2014- Research Assistant, Institute of Machine Tools and Manufacturing (IWF), ETH Zürich

Main Works:
• N. Lanz, D. Spescha, N. Ceresa, A. Ryser, and S. Weikert, "Modelling and Validation of Position Dependant Structural Deformations of a Machine Tool Structure under Gravitational Loads," euspen 17th Int. Conf. & Exhibition, 2017.

Name:
Daniel Spescha

Affiliation:
Research Assistant, inspire AG

Address:
Technoparkstrasse 1, 8005 Zürich, Switzerland

Brief Biographical History:
2011 Received Master of Science in Engineering from Zentralstelle für Fernstudien an Fachhochschulen (ZFH)
2011- Research Assistant and Doctoral Student, inspire AG

Main Works:
• D. Spescha, S. Weikert, O. Zirn, and K. Wegener, "Synchronisation of feed axes with differing bandwidths using set point delay," Int. J. Automation Technol., Vol.11, No.2, pp. 155-164, 2017.

Name:
Sascha Weikert

Affiliation:
Group Leader Simulation, inspire AG

Address:
Technoparkstrasse 1, 8005 Zürich, Switzerland

Brief Biographical History:
2000 Received Ph.D. from ETH Zürich
2000- Institute for Machine Tools and Manufacturing (IWF), ETH Zürich
2016- inspire AG

Main Works:
• "Thermal behavior improvement of linear axis," Proc. of the 11th euspen Conf., Como, Italy, 2011.
• "Evaluation of modelling approaches for machine tool design," Precision Engineering, Vol.34, pp. 399-407, 2010.
• "R-Test, a new device for accuracy Measurements on five axis machine tools," CIRP Vol.53, No.1, pp. 429-432, 2004.

Membership in Academic Societies:
• American Society of Precision Engineering (ASPE)
• European Society for Precision Engineering and Nanotechnology (euspen)

Name:
Konrad Wegener

Affiliation:
Professor, Institute of Machine Tools and Manufacturing (IWF), ETH Zürich

Address:
Leonhardstrasse 21, 8092 Zürich, Switzerland

Brief Biographical History:
1991- Ph.D., Technische Universität Braunschweig
1999- Head, Design and Layout Planning Departments at Schuler Presses GmbH & Co. KG
2003- CEO, Schuler Held Lasertechnik GmbH & Co. KG
2003- Head, Institute of Machine Tools and Manufacturing (IWF), ETH Zürich
2011- CEO, Mechatronic Production Systems and Manufacturing, inspire AG

Main Works:
• "Conditioning and Monitoring of Grinding Wheels," CIRP, Vol.60, No.2, pp. 757-777, 2011.
• "Phenomenological Compensation of Thermally caused Position and Orientation Errors of Rotary Axes," J. of Manufacturing Processes, Vol.15, No.4, pp. 452-459, 2013.
• "Optimal control for chatter mitigation in milling, Part 1: Modelling and control design," Control Engineering Practice, Vol.24, pp. 155-166, 2014.
• "Optimal control for chatter mitigation in milling, Part 2: Experimental validation," Control Engineering Practice, Vol.24, pp. 167-175, 2014.
• "Open Loop Inertial Cross-talk Compensation Based on Measurement Data," 25th Annual Meeting of The American Society for Precision Engineering, 2010, Atlanta, USA, 2010.

Membership in Academic Societies:
• International Academy for Production Engineering (CIRP), Associate Member